


Effect of neutron excess in the entrance channel on the $^{18}\text{O} + ^{93}\text{Nb}$ system: An experimental study relevant to incomplete-fusion dynamics

Avinash Agarwal ^{*}, Anuj Kumar Jashwal, Munish Kumar, and S. Prajapati
Department of Physics, Bareilly College, Bareilly (U.P.)-243 005, India

Sunil Dutt , Muntazir Gull, and I. A. Rizvi
Department of Physics, Aligarh Muslim University, Aligarh (U.P.)-202 002, India


Kamal Kumar
Department of Physics, Hindu College, Moradabad (U.P.)-244 001, India

Sabir Ali 
MANUU Polytechnic Darbhanga, Maulana Azad National Urdu University, Hyderabad -500 032, India

Abhishek Yadav
Department of Physics, Jamia Millia Islamia, New Delhi- 110 025, India

Rakesh Kumar
NP-Group, Inter University Accelerator Center, New Delhi-110 067, India

A. K. Chaubey
Department of Physics, Addis Ababa University, P.O. Box 1176, Addis Ababa, Ethiopia

 (Received 1 September 2020; accepted 18 February 2021; published 2 March 2021)

The incomplete fusion dynamics in the $^{18}\text{O} + ^{93}\text{Nb}$ system at energies above the Coulomb barrier has been investigated. The experimentally measured cross sections have been compared with the theoretical predictions of the statistical model code PACE4. To examine the effect of entrance channel parameters on the onset and strength of incomplete fusion, relative contributions of complete and incomplete fusion have been deduced from the analysis of measured excitation functions. The contribution of incomplete fusion deduced from the analysis of excitation functions has been studied in terms of various entrance channel parameters, namely, entrance channel mass asymmetry (μ_A) of interacting projectile and target combination, Coulomb factor ($Z_P Z_T$), ground state α - Q value of the reaction, and neutron skin thickness of target nuclei. It has been found that the probability of incomplete fusion depends strongly on entrance channel parameters. Further, the incomplete fusion contribution for the ^{18}O projectile with two excess neutrons is noticed to be relatively larger as compared to ^{16}O . This may be due to the larger probability of breakup for the ^{18}O projectile resulting in rather weak binding forces as compared to ^{16}O . The existence of incomplete fusion below critical angular momentum (ℓ_{crit}), i.e., $\ell \leq \ell_{\text{crit}}$, has also been observed for the studied system.

DOI: [10.1103/PhysRevC.103.034602](https://doi.org/10.1103/PhysRevC.103.034602)

I. INTRODUCTION

In recent years, fusion reactions induced by heavy ions (HIs) have been one of the main research areas in low energy nuclear physics [1–4]. Complete fusion (CF) and incomplete fusion (ICF) reactions are the most dominant reaction mechanisms at energies near and above the Coulomb barrier [5–8]. When just one of the breakup fragments fuses with the target, we employ the term ICF, whereas all fragments are absorbed by the target is named CF. The first experimental confirmation

of projectile-like fragments (PLFs) in such reaction process was reported by Britt and Quinton [9]. In order to understand the underlying reaction dynamics, different type of models has been proposed to explain the onset of ICF at low incident energies. The SUMRULE model given by Wilczynski *et al.* [10] suggested that ICF is especially confined to the ℓ -space above ℓ -critical value (ℓ_{crit}) for CF and originate from peripheral interactions or non-central collisions. The noncentral nature of ICF reaction dynamics has also been emphasized by Trautmann *et al.* [11], and Inamura *et al.* [12,13]. Other theoretical models, viz., the breakup fusion (BUF) model [14], the promptly emitted particle model [15], the exciton models [16], etc., have been proposed to explain various characteristics of

^{*} avibcb@gmail.com

ICF. In fact, none of these models is able to explain satisfactorily the ICF reaction dynamics at lower energies below 10 MeV/nucleon. The development of a theoretical model to elucidate ICF dynamics remained elusive and continues to be an active area of investigation at low incident energies.

During the last few decades, efforts have been made to understand the dynamics of ICF at energies just above the Coulomb barrier and their dependence on various entrance channel parameters [17–22]. Recently, it has also been observed that ICF becomes more and more dominant as the projectile energy increases [23–26]. Morgenstern *et al.* [27] have associated the ICF fraction with entrance-channel mass asymmetry. In their work, Shuaib *et al.* [28] suggested that ICF probability follows a systematic linear growth with respect to the charge product $Z_P Z_T$ (Coulomb factor). Further, systematic studies have also been done by Tali *et al.* [29] and Harish *et al.* [30] suggest that ICF behavior with Coulomb factor follows linear trends but separately for each projectile. Neutron skin thickness deals with neutron-proton radii differences [31]. It would be interesting to see the neutron skin thickness for neutron rich nuclei and its dependency on ICF. In addition to recent studies [20,28,32] performed on ICF dynamics with several entrance channel parameters, it would also be interesting to probe the effect of α -separation energy on ICF dynamics. To know the onset of ICF, its effect on CF and various entrance channel parameters, the excitation functions (EFs) of evaporation residues (ERs) populated in the $^{18}\text{O} + ^{93}\text{Nb}$ system has been studied. The work reported in the article has been carried out by employing the off-beam activation technique followed by γ ray spectroscopy, in which direct detection of α s and protons (or projectile-like fragments) is not possible. However, some studies are available in literature, where authors have measured kinetic energy spectra and angular distribution of projectile-like fragments including protons and α s in order to estimate experimentally the importance of the ICF process [33–35]. Furthermore, to probe the importance of ICF dynamics, the experimental detection of α s and protons is possible by an in-beam coincidence measurement of spin distribution of the reaction residues [36,37]. The measured EFs are then compared with theoretical predictions obtained by employing the statistical model code PACE4 [38]. Present data along with those available in literature have been studied to get an unambiguous dependency of ICF on various entrance channel parameters, namely, entrance channel mass asymmetry (μ_A) of the interacting partners, Coulomb factor ($Z_P Z_T$, where Z_P and Z_T are the atomic numbers of projectile and target, respectively), ground state α - Q value of the reaction, and neutron skin thickness of the target.

II. EXPERIMENTAL PROCEDURE

The present experiments have been carried out using the 15UD pelletron accelerator facility at Inter-University Accelerator Center (IUAC), New Delhi, India. Self-supporting targets of ^{93}Nb having thickness ≈ 1.4 – 1.5 mg/cm² and aluminum (Al) catcher foils of thickness ranging from 0.8 to 1.6 mg/cm² were prepared by a rolling technique. The thickness and uniformity of each target and catcher foil has been verified by an α -transmission method as well as by microbal-

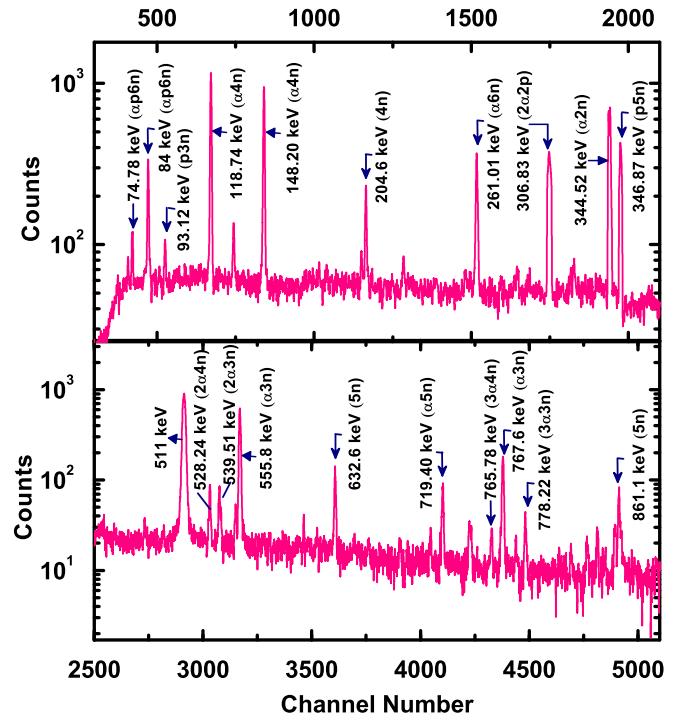


FIG. 1. Typical γ -ray energy spectrum obtained from the interaction of the $^{18}\text{O} + ^{93}\text{Nb}$ system at $E_{\text{lab}} = 92.2$ MeV energy. Some of the identified γ -ray peaks have been assigned to their respective evaporation residues populated via CF and/or ICF channels.

ance. Two stacks each composed of five ^{93}Nb foils backed with aluminum (Al) foils were irradiated in two individual runs. The Al backing of the targets served as the energy degrader as well as the catcher to trap the recoiling residues produced during irradiation. According to the half-life of the main isotopes produced during irradiation, each stack was irradiated for about seven hours in the General Purpose Scattering Chamber (GPSC), which has an in-vacuum transfer facility. A Faraday cup was installed downstream of the scattering chamber to monitor the beam current. The activities induced in the catcher assembly were followed off-line, using a precalibrated high-purity germanium (HPGe) detector coupled with the computer automated measurement and control (CAMAC) based acquisition system CANDLE software developed by the IUAC [39]. After the end of irradiation, the target and its associated catcher were taken from the GPSC chamber and placed in between two HPGe detectors positioned 180° to each other. The Ge crystal of detector and target-Al foils was surrounded by a thick Pb shield to reduce scattered γ rays from the neighboring target and background from natural radioactivity. The absolute efficiencies of the detectors were determined by employing a ^{152}Eu source mounted at the same geometry and absorption conditions as the target-Al foils. The energy resolution of the HPGe detector was found to be 2.5 keV for 1408 keV γ ray for a standard ^{152}Eu source. The incident beam energy on each target and catcher foil has been calculated by the code SRIM (Stopping and Range of Ions in Matter) [40]. The γ ray spectrum recorded at $E_{\text{lab}} = 92.2 \pm 1.3$ MeV is shown in Fig. 1. The various ERs populated in the present

TABLE I. List of identified reaction residues in the $^{18}\text{O} + ^{93}\text{Nb}$ system and their decay data.

Residues(s)	Spin	Half-life	E_γ (keV)	I_γ (%)
$^{108}\text{In}(3n)$	7^+	58 min	242.6	41
$^{107}\text{In}(4n)$	$9/2^+$	32.4 min	204.6	47.2
$^{106}\text{In}(5n)$	7^+	6.2 min	632.6	99.7
			861.1	99
$^{107}\text{Cd}(p3n)$	$5/2^+$	6.5 h	93.12	4.7
$^{105}\text{Cd}(p5n)$	$5/2^+$	55.5 min	346.87	4.2
$^{105}\text{Ag}(\alpha 2n)$	$1/2^-$	41.29 d	344.52	41.4
$^{104}\text{Ag}(\alpha 3n)$	5^+	69.2 min	555.8	92.6
			767.6	65.7
$^{103}\text{Ag}(\alpha 4n)$	$7/2^+$	65.7 min	118.74	31.2
			148.20	28.3
$^{102}\text{Ag}(\alpha 5n)$	5^+	12.9 min	719	58
$^{101}\text{Ag}(\alpha 6n)$	$9/2^+$	11.1 min	261.01	52.6
$^{100}\text{Pd}(\alpha p6n)$	0^+	3.63 d	84	52
			74.78	48
$^{100}\text{Rh}(2\alpha 3n)$	1^-	20.8 h	539.51	80.6
$^{99}\text{Rh}(2\alpha 4n)$	$1/2^-$	16.1 d	528.24	37.9
$^{101}\text{Tc}(2\alpha 2p)$	$9/2^+$	14.22 min	306.83	89
$^{96}\text{Tc}(3\alpha 3n)$	7^+	4.28 d	778.22	99.76
$^{95}\text{Tc}(3\alpha 4n)$	$9/2^+$	20 h	765.78	93.8

work have been identified not only by their characteristic γ ray energies, but also by their decay profiles and branching ratios. The nuclear spectroscopic data used in the evaluations and measurement of cross sections have been taken from the Table of Radioactive Isotopes [41] and are listed in Table I. The standard formulation, as adopted in Ref. [42], has been used to determine the production cross section of various reaction products. Errors in the measured ER cross sections include systematic uncertainties that could arise from different sources, such as (i) the nonuniformity in the thickness of the sample may lead to uncertainty in determination of number of target nuclei. It is estimated that the error in the thickness of sample materials is less than 1%. (ii) The uncertainty in the efficiency calibration of the HPGe detector has been estimated to be less than 2%. (iii) Fluctuations in the beam current may result in the variation of incident flux, proper care has been taken to maintain the beam current constant. The weighted average of the beam current has been taken to estimate the errors due to this factor, which is found to be less than 2%. (iv) To minimize the error, the counting has been done for a dead time below 10%. (v) Uncertainty due to the straggling effect of the projectile passing through the stack has been estimated to be less than 2%. Efforts are made to minimize the uncertainty associated with the various sources. The general errors in the present work have been estimated to be $\leq 17\%$.

III. OBTAINED RESULTS, ANALYSIS, AND THEIR INTERPRETATION

In this paper, excitation functions of 16 ERs, namely, $^{108}\text{In}(3n)$, $^{107}\text{In}(4n)$, $^{106}\text{In}(5n)$, $^{107}\text{Cd}(p3n)$, $^{105}\text{Cd}(p5n)$, $^{105}\text{Ag}(\alpha 2n)$, $^{104}\text{Ag}(\alpha 3n)$, $^{103}\text{Ag}(\alpha 4n)$, $^{102}\text{Ag}(\alpha 5n)$, $^{101}\text{Ag}(\alpha 6n)$, $^{100}\text{Pd}(\alpha p6n)$, $^{100}\text{Rh}(2\alpha 3n)$, $^{99}\text{Rh}(2\alpha 4n)$,

$^{101}\text{Tc}(2\alpha 2p)$, $^{96}\text{Tc}(3\alpha 3n)$, and $^{95}\text{Tc}(3\alpha 4n)$ are found to be populated through different fusion processes in the $^{18}\text{O} + ^{93}\text{Nb}$ system at projectile energies $\approx 3.5\text{--}5.5$ MeV/A. The analysis of EFs has been carried out in the light of well-established statistical model code PACE4, which follows the Monte Carlo simulation procedure for the de-excitation of the compound nucleus (CN). PACE4 is based on the Hauser-Feshbach theory of CN decay [43]. The angular momentum projections are calculated at each stage of de-excitation.

The transmission coefficients for the light emitted particles like neutrons (n), protons (p), and alpha (α) during the de-excitation of excited CN are obtained by optical model calculations. The Bass model is employed to estimate the input fusion cross section of evaporation residues [44]. In this code, the level density parameter is defined by the relation $a = A/K$, where A is the mass of CN and K is an adjustable parameter which is used to reproduce the experimentally measured EFs. However, it has been observed that the code PACE4 does not take ICF into account. Hence, the enhancement in the experimental cross sections over the theoretical predictions give a clear indication of the incomplete fusion process. Measured cross section data are presented in Tables II and III. The evaporation residues produced through various reaction channels in the $^{18}\text{O} + ^{93}\text{Nb}$ system are discussed below.

A. Excitation function measurement of xn and pxn emitting channels

The experimentally measured EFs of $^{108}\text{In}(3n)$, $^{107}\text{In}(4n)$, $^{106}\text{In}(5n)$, $^{107}\text{Cd}(p3n)$, and $^{105}\text{Cd}(p5n)$ are populated through the emission of xn and pxn channels. These ERs have been observed without any precursor contributions. In order to optimize the level density parameter K , the experimentally measured EFs are compared with PACE4 predictions for different K values ($K = 8, 10, \text{ and } 12$). As a representative case, the effect of variation of the parameter K on measured EFs is reported in Fig. 2(a). As can be inferred from Figs. 2 and 3, the experimentally measured excitation functions of the ERs $^{108}\text{In}(3n)$, $^{107}\text{In}(4n)$, $^{106}\text{In}(5n)$, $^{107}\text{Cd}(p3n)$, and $^{105}\text{Cd}(p5n)$ with $K = 12$ for the $^{18}\text{O} + ^{93}\text{Nb}$ system are found to be in good agreement for the present experimental data over a broad energy range. The choice of parameter $K = 12$ has also been adopted by Maiti in her work and is justified [45].

Further, from Fig. 3(b), it can be seen that the reported values of $\Sigma\sigma_{xn+pxn}^{\text{exp}}$ are compared with those predicted by PACE4 code ($\Sigma\sigma_{xn+pxn}^{\text{PACE4}}$) for the same ERs populated via xn and pxn channels at free parameter value $K = 12$. It may be pointed out from this figure that the PACE4 code significantly reproduces the sum of experimentally measured cross sections within the range of error bars. This once more proves that the ERs $^{108}\text{In}(3n)$, $^{107}\text{In}(4n)$, $^{106}\text{In}(5n)$, $^{107}\text{Cd}(p3n)$, and $^{105}\text{Cd}(p5n)$ are produced only with CF. Thus, the choice of parameters used for the analysis is suitable, and therefore the value of level density $a = A/12$ MeV $^{-1}$ can be used consistently as an optimized parameter for the analysis of the reaction channels expected to be populated via both CF and ICF reaction processes.

TABLE II. Experimentally measured production reaction cross sections of the evaporation residues ^{108}In , ^{107}In , ^{106}In , ^{107}Cd , and ^{105}Cd populated in the $^{18}\text{O} + ^{93}\text{Nb}$ system.

E_{lab} (MeV)	$\sigma(^{108}\text{In})$ (mb)	$\sigma(^{107}\text{In})$ (mb)	$\sigma(^{106}\text{In})$ (mb)	$\sigma(^{107}\text{Cd})$ (mb)	$\sigma(^{105}\text{Cd})$ (mb)
99.20 ± 1.3	–	14.65 ± 2.49	162.04 ± 27.54	–	152.9 ± 25.99
92.19 ± 1.3	–	45.42 ± 7.72	207.01 ± 35.19	38.78 ± 6.59	57.03 ± 9.69
89.28 ± 1.3	–	84.64 ± 14.38	212.67 ± 36.15	52 ± 8.84	18.76 ± 3.19
84.85 ± 1.2	4.63 ± 0.69	145.13 ± 24.67	178.55 ± 30.35	120.58 ± 20.49	–
82.30 ± 1.2	6.42 ± 0.96	188.79 ± 32.09	138.91 ± 36.15	135.51 ± 23.03	–
76.84 ± 1.3	17.71 ± 2.65	288 ± 48.96	63.77 ± 10.84	199 ± 33.83	–
72.33 ± 1.3	39.06 ± 5.86	324.91 ± 55.23	–	188.29 ± 32.01	–
68.37 ± 1.2	90.24 ± 13.53	278.27 ± 47.30	–	146.66 ± 24.93	–
61.56 ± 1.3	182.91 ± 27.43	104.81 ± 17.81	–	–	–

Furthermore, to verify the accuracy in our measurement an effort has been made to deduce the value of the fusion barrier (V_{CB}) from the analysis of experimentally measured CF excitation functions. According to Gutbrod *et al.* [46], the normalized CF probability may be given as

$$\sigma_{CF} = \pi R_{\text{int}}^2 (1 - V_{CB}/E_{c.m.}).$$

The value of $\Sigma\sigma_{CF}$ is plotted as a function of $1/E_{\text{lab}}$ in Fig. 4. As can be seen in this figure, the $\Sigma\sigma_{CF}$ data points indicate a linear curve that intersects the x axis at the beam energy equal to V_{CB} within the range of error bars. This confirms the value of the fusion barrier ($V_{CB} \approx 51.16$ MeV) for the $^{18}\text{O} + ^{93}\text{Nb}$ system and provides confidence in our measurement.

B. Excitation function measurement for the αxn , αpxn , $2\alpha xn$, $2\alpha xp$, and $3\alpha xn$ emitting channels

The experimentally measured excitation functions of 11 ERs populated via αxn , αpxn , $2\alpha xn$, $2\alpha xp$, and $3\alpha xn$ emission channels, namely, $^{105}\text{Ag}(\alpha 2n)$, $^{104}\text{Ag}(\alpha 3n)$, $^{103}\text{Ag}(\alpha 4n)$, $^{102}\text{Ag}(\alpha 5n)$, $^{101}\text{Ag}(\alpha 6n)$, $^{100}\text{Pd}(\alpha p6n)$, $^{100}\text{Rh}(2\alpha 3n)$, $^{99}\text{Rh}(2\alpha 4n)$, $^{101}\text{Tc}(2\alpha 2p)$, $^{96}\text{Tc}(3\alpha 3n)$, and $^{95}\text{Tc}(3\alpha 4n)$ are displayed in Figs. 5–7. Due to the involvement of α emission in the exit channel, these ERs are supposed to be populated via ICF in addition to the CF process. It is also important to say that the experimentally measured cross sections for the ERs ^{105}Ag ($t_{1/2} = 41.29$ d) populated through the emission of the $(\alpha 2n)$ channel is strongly fed from its precursor ^{105}Cd ($t_{1/2} = 55.5$ min). The independent cross sections (σ_{ind}) have been estimated from the cumulative cross

TABLE III. Experimentally measured production reaction cross sections of the evaporation residues ^{105}Ag , ^{104}Ag , ^{103}Ag , ^{102}Ag , ^{101}Ag , ^{100}Pd , ^{100}Rh , ^{99}Rh , ^{101}Tc , ^{96}Tc , and ^{95}Tc populated in the $^{18}\text{O} + ^{93}\text{Nb}$ system.

E_{lab} (MeV)	$\sigma^{\text{ind}}(^{105}\text{Ag})$ (mb)	$\sigma(^{104}\text{Ag})$ (mb)	$\sigma(^{103}\text{Ag})$ (mb)	$\sigma(^{102}\text{Ag})$ (mb)	$\sigma(^{101}\text{Ag})$ (mb)	$\sigma(^{100}\text{Pd})$ (mb)
99.20 ± 1.3	96.12 ± 16.34	142.14 ± 24.16	394.28 ± 67.02	136.72 ± 23.24	53.64 ± 9.11	33.27 ± 5.65
92.19 ± 1.3	56.5 ± 9.60	183.25 ± 31.15	353.6 ± 60.11	33.79 ± 5.74	35.74 ± 6.07	29.40 ± 4.99
89.28 ± 1.3	21.49 ± 3.65	259.13 ± 44.05	281.64 ± 47.88	20.47 ± 3.48	25.60 ± 4.35	26.77 ± 4.55
84.85 ± 1.2	–	260 ± 44.2	199.38 ± 33.89	–	11.92 ± 2.02	23.29 ± 3.96
82.30 ± 1.2	–	241.75 ± 41.09	159.16 ± 27.05	–	–	22.92 ± 3.89
76.84 ± 1.3	–	216.58 ± 36.81	76.61 ± 13.02	–	–	22.23 ± 3.77
72.33 ± 1.3	–	186.99 ± 31.78	18.49 ± 3.14	–	–	21.40 ± 3.63
68.37 ± 1.2	–	145.40 ± 24.71	–	–	–	20.27 ± 3.44
61.56 ± 1.3	–	45.77 ± 7.78	–	–	–	19.56 ± 3.32
E_{lab} (MeV)	$\sigma(^{100}\text{Rh})$ (mb)	$\sigma(^{99}\text{Rh})$ (mb)	$\sigma(^{101}\text{Tc})$ (mb)	$\sigma(^{96}\text{Tc})$ (mb)	$\sigma(^{95}\text{Tc})$ (mb)	
99.20 ± 1.3	133.61 ± 22.71	78.34 ± 13.31	9.02 ± 1.53	43.74 ± 7.43	74.71 ± 12.70	
92.19 ± 1.3	99.37 ± 16.89	26.17 ± 4.44	7.29 ± 1.23	46.19 ± 7.85	80.95 ± 13.76	
89.28 ± 1.3	65.56 ± 11.14	17.24 ± 2.93	5.69 ± 0.96	45.76 ± 7.77	74.65 ± 12.69	
84.85 ± 1.2	46.39 ± 7.88	5.30 ± 0.90	3.26 ± 0.55	45.27 ± 7.69	55.3 ± 9.40	
82.30 ± 1.2	25.98 ± 4.41	–	–	43.39 ± 7.37	50.03 ± 8.50	
76.84 ± 1.3	–	–	–	37.71 ± 6.41	30.99 ± 5.26	
72.33 ± 1.3	–	–	–	–	15.79 ± 2.68	
68.37 ± 1.2	–	–	–	–	15.15 ± 2.57	
61.56 ± 1.3	–	–	–	–	–	

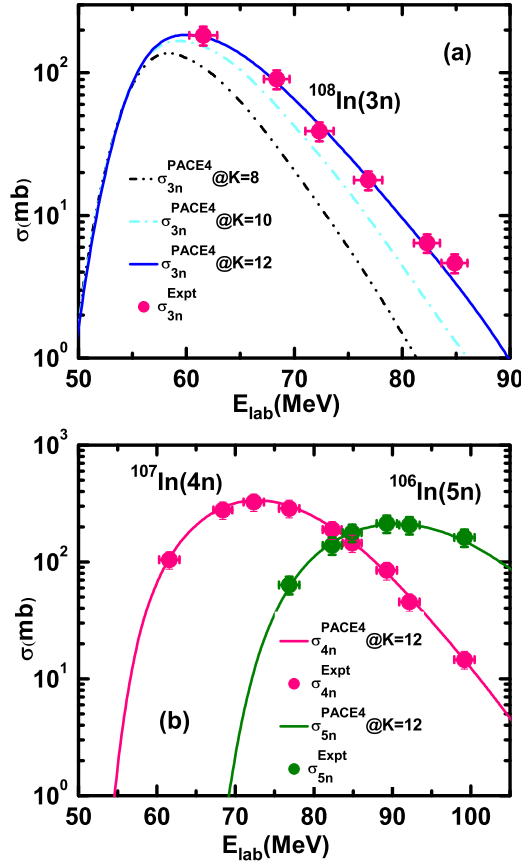


FIG. 2. (a) Experimentally measured EFs of evaporation residue $^{108}\text{In}(3n)$ along with PACE4 calculations ($K = 8, 10,$ and 12). (b) Experimentally measured EFs of evaporation residues $^{107}\text{In}(4n)$ and $^{106}\text{In}(5n)$ along with PACE4 calculations ($K = 12$).

sections (σ_{cum}) by using the Cavinato *et al.* [47] formulation given as

$$\sigma_{\text{ind}} = \sigma_{\text{cum}} - P_{\text{pre}} \left[\frac{t_{1/2}^D}{t_{1/2}^D - t_{1/2}^P} \right] \sigma_P.$$

Here, σ_P is the cross section of parent nuclei, while $t_{1/2}^D$ and $t_{1/2}^P$ are the half-lives of the daughter and precursor nuclei. The P_{pre} is the branching ratio of the precursor to its daughter nuclei. The independent cross section of ^{105}Ag has been evaluated using the following expression:

$$\sigma_{\text{ind}}^{105\text{Ag}} = \sigma_{\text{cum}}^{105\text{Ag}} - 1.0009 \sigma_{\text{ind}}^{105\text{Cd}}.$$

The values of σ_{ind} and σ_{cum} for $^{105}\text{Ag}(\alpha 2n)$ are shown in Fig. 5(a). The experimentally measured cross sections for these ERs have been compared with the theoretical predictions of the PACE4 code at level density parameter $a = A/12 \text{ MeV}^{-1}$. It can be seen from these figures, the enhancement observed in the experimental cross sections over the theoretically predicted cross sections indicate the occurrence of the third variety of the reaction process, which is not considered in the PACE4 code. It might be due to breakup fusion,

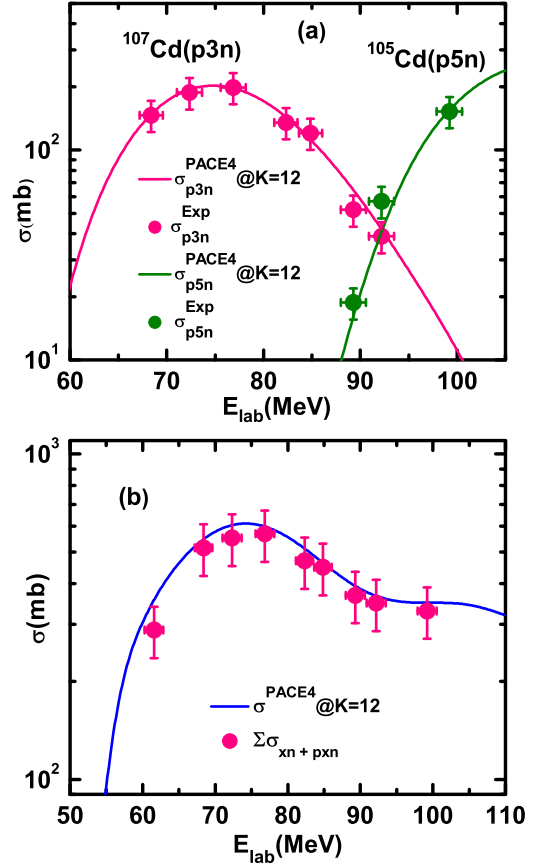


FIG. 3. (a) Experimentally measured EFs of all pxn ($x = 3$ and 5) channels. (b) Sum of all CF channels along with PACE4 calculations ($K = 12$).

generally called partial fusion or ICF. As a representative case, the mode of formation of ^{99-x}Tc residual isotopes, which may be populated both via complete fusion and/or incomplete fusion reaction channels are given below.

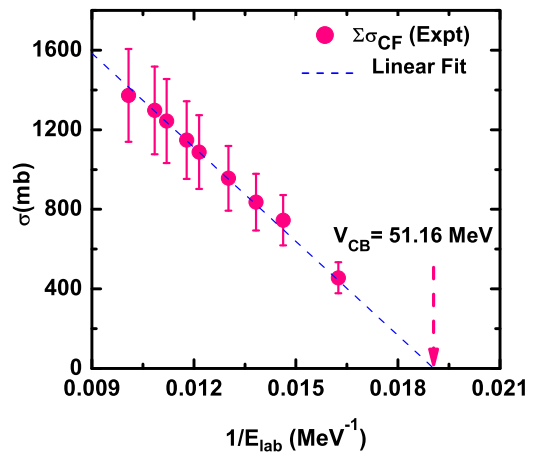


FIG. 4. CF cross section as a function of $1/E_{\text{lab}}$ found to reproduce the Coulomb barrier for the $^{18}\text{O} + ^{93}\text{Nb}$ system. The dashed line through the data point is achieved by a best-fitting producer on the data point.

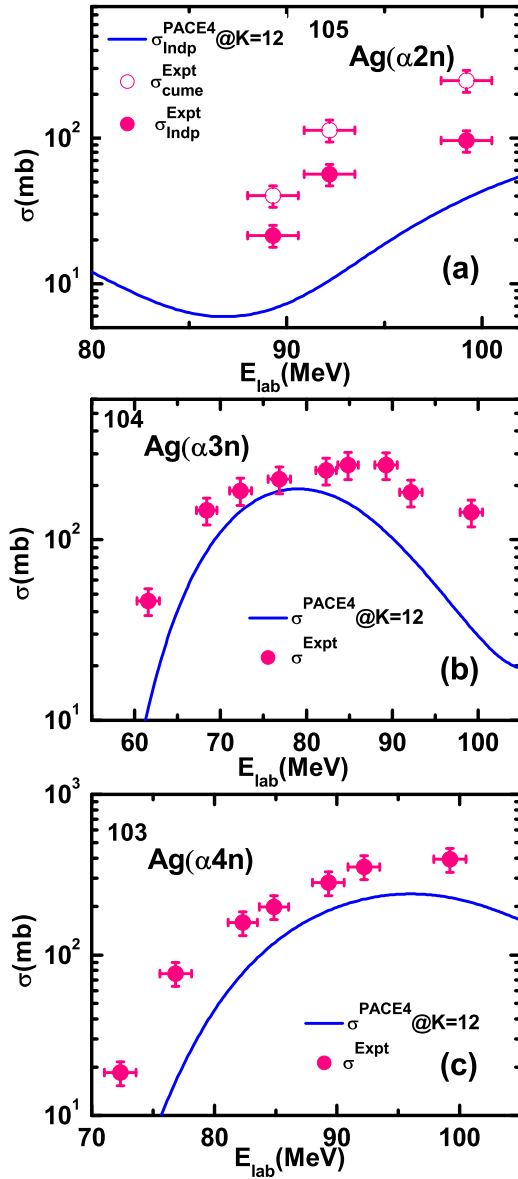
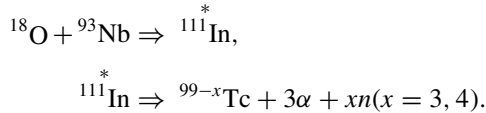
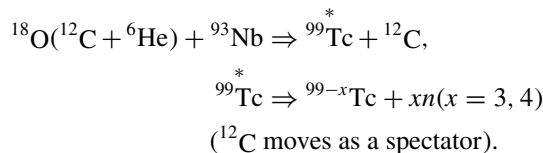


FIG. 5. Experimentally measured EFs ^{105}Ag , ^{104}Ag , and ^{103}Ag panels [(a)–(c)] are compared with PACE4 predictions ($K = 12$). Hollow symbol represents the measured cumulative cross section.

(a) CF of ^{18}O with ^{93}Nb :



(b) ICF of ^{18}O with ^{93}Nb :



However, Figs. 6(b) and 7(a), (d), (e), (f) show the experimental EFs of ^{101}Ag , ^{100}Pd , ^{101}Tc , ^{96}Tc , and ^{95}Tc residues,

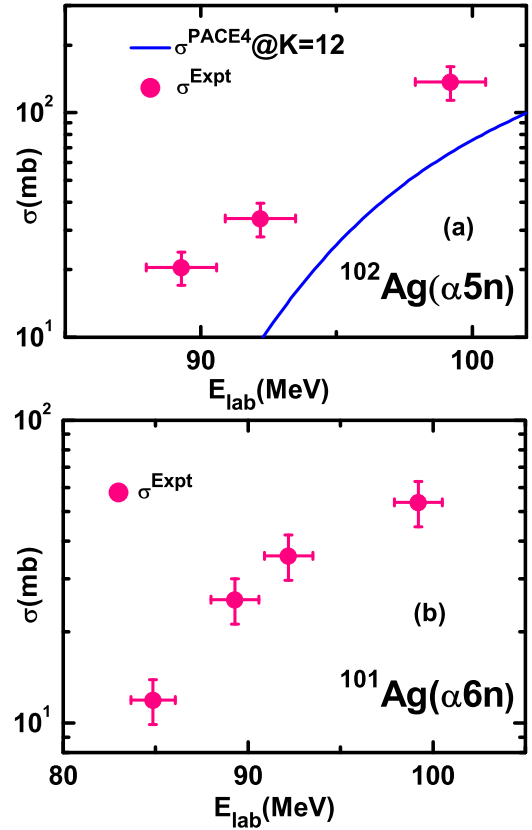


FIG. 6. Experimentally measured EFs ^{102}Ag and ^{101}Ag are compared with PACE4 predictions ($K = 12$).

where the theoretical predictions of the code PACE4 predict the negligible cross sections and here are not shown. This indicates the contribution for these residues is via only the ICF process.

IV. EFFECT OF ENTRANCE CHANNEL PARAMETERS ON ICF

The contribution of ICF in α -particle emitting channels has been deduced as $\Sigma\sigma_{ICF} = \Sigma\sigma_{\text{exp}} - \Sigma\sigma_{\text{PACE4}}$, i.e., by subtracting the PACE4 cross-section values from all α -emitting channels from their corresponding experimentally measured values at the studied energy range. It is worth mentioning that in the present work the extraction of the ICF contribution is justified, as the code PACE4 reproduces well the cross sections of the residues for xn and pxn reaction channels formed by the CF process. By fixing the same set of the parameters of the code PACE4, the observed enhancement in the experimental cross section with respect to model calculations for α emitting reaction channels is attributed to the contribution of ICF process. To clarify the ICF contribution to the total fusion (TF) cross section ($\sigma_{TF} = \Sigma\sigma_{CF} + \Sigma\sigma_{ICF}$), the sum of the CF cross sections of all channels ($\Sigma\sigma_{CF}$), $\Sigma\sigma_{ICF}$, and σ_{TF} are plotted as a function of incident projectile energy in Fig. 8. However, in the present case the calculated TF, CF, and ICF cross sections differ markedly, indicating the importance of incident projectile energy on the fusion

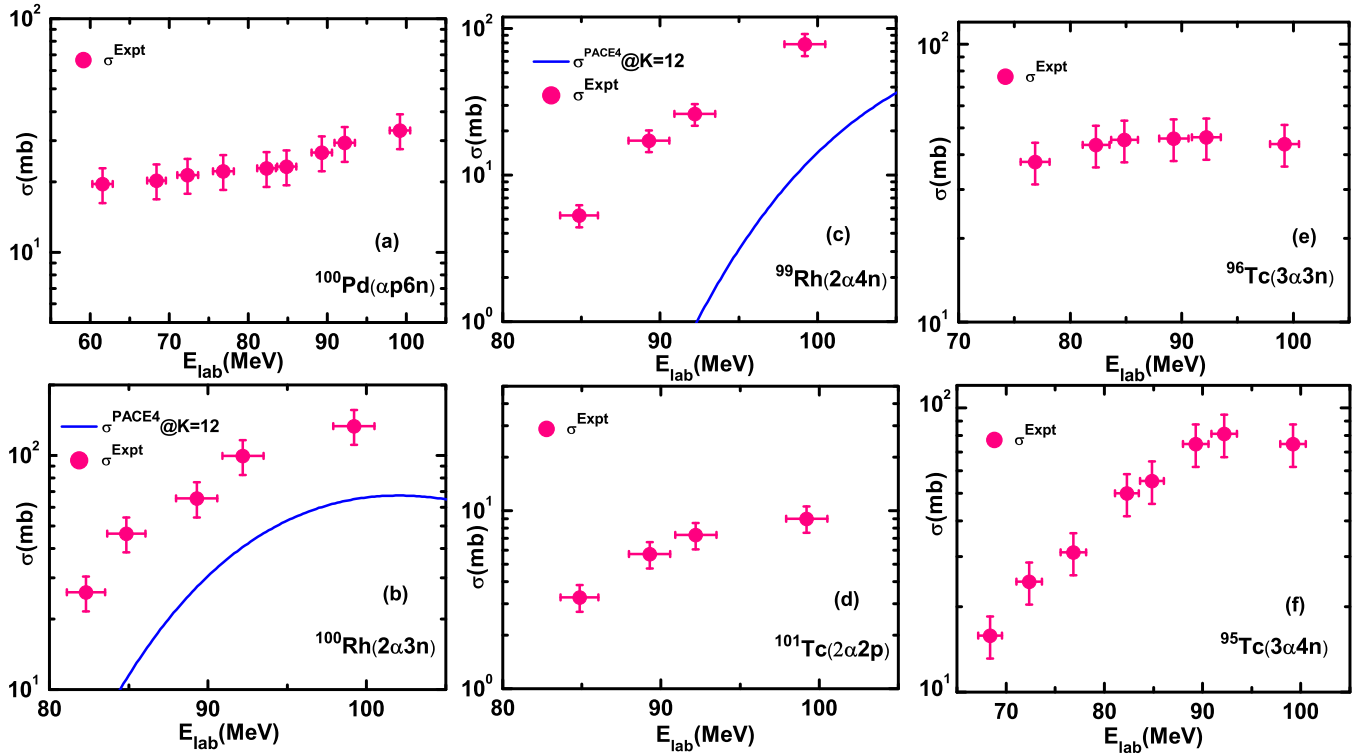


FIG. 7. Experimentally measured EFs ^{100}Pd , ^{100}Rh , ^{99}Rh , ^{101}Tc , ^{96}Tc , and ^{95}Tc are compared with PACE4 predictions ($K = 12$).

dynamics for the studied system. On increasing incident projectile energy, the separation between σ_{CF} and σ_{TF} also increases. The increasing trend of the ICF fraction or probability of ICF, $F_{ICF}(\%)$ [$F_{ICF}(\%) = (\Sigma\sigma_{ICF}/\sigma_{TF}) \times 100$], with increasing projectile energies has been observed in the $^{18}\text{O} + ^{93}\text{Nb}$ system, which is given in the inset of Fig. 8. The ICF fraction [$F_{ICF}(\%)$] is a measure of the strength of

incomplete fusion relative to the total fusion. It is worth mentioning that some of the reaction channels could not be identified due to their short half-lives of the residual radionuclides or production of stable isotopes. Thus, the computed ICF cross section may be considered as the lower limit of ICF for the $^{18}\text{O} + ^{93}\text{Nb}$ system.

A. ICF dependence on incident beam energy

In order to review the dependence of $F_{ICF}(\%)$ on incident projectile energy, the $F_{ICF}(\%)$ has been measured for the present system $^{18}\text{O} + ^{93}\text{Nb}$ and compared with the $F_{ICF}(\%)$ for the other systems, namely, $^{18}\text{O} + ^{159}\text{Tb}$ [4], $^{18}\text{O} + ^{175}\text{Lu}$ [48]. The comparison has been plotted against the normalized relative velocity (V_{rel}/c) as shown in Fig. 9. The following expression has been used for the calculation of relative velocity:

$$V_{rel} = \sqrt{2(E_{c.m.} - V_{CB})/\mu},$$

where μ is the reduced mass of the system and $E_{c.m.}$ is the center of mass energy for the reaction. From this figure, it is clear that for the $^{18}\text{O} + ^{93}\text{Nb}$ system the $F_{ICF}(\%)$ is found to be $\approx 2\%$ at energy 25% above the barrier which increases up to $\approx 19\%$ at the energy around 59% above the Coulomb barrier. Similarly, the $F_{ICF}(\%)$ for other systems also increases with an increase in the incident projectile energy. It can also be observed from Fig. 9, that for the nearly same value of relative velocity, the order of magnitude of $F_{ICF}(\%)$ is less for Nb than for Tb and Lu targets. Hence, the present results indicate that additionally to the incident projectile beam energy, some more entrance channel parameters are required to explore ICF dynamics for a wide range of mass nuclei at low energies.

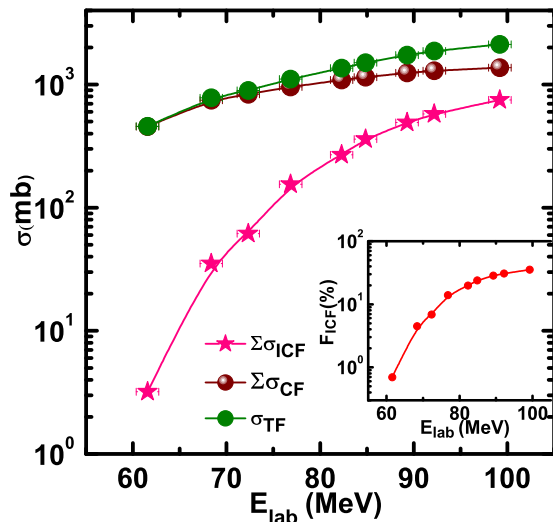


FIG. 8. The total fusion cross section σ_{TF} along with the sum of complete fusion and incomplete fusion cross section ($\Sigma\sigma_{CF}$ and $\Sigma\sigma_{ICF}$), and in the inset the probability of incomplete fusion, are plotted as a function of incident projectile energy.

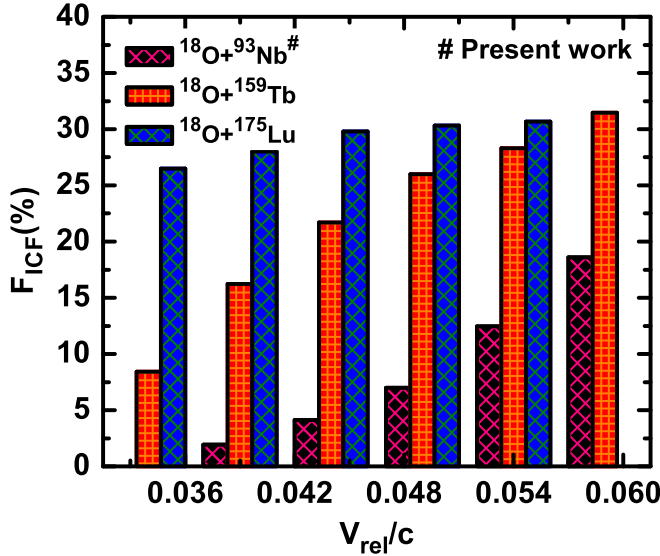


FIG. 9. The comparison of deduced $F_{ICF}(\%)$ as a function of normalized relative velocity (V_{rel}/c) for ^{18}O projectile on different targets. For references and details see text.

B. ICF dependence on mass asymmetry

According to the mass-asymmetry systematics of Morgenstern *et al.* [27] that at a given V_{rel} the ICF fraction increases with an increase in mass asymmetry (μ_A) of the projectile-target combination. So in order to check the consistency of the Morgenstern *et al.* [27] mass-asymmetry systematics, the value of the ICF fraction for the present system $^{18}\text{O} + ^{93}\text{Nb}$ has been compared with those obtained for the ^{18}O induced reaction with ^{159}Tb [4] and ^{175}Lu [48] targets, ^{16}O induced reaction with ^{93}Nb [49], ^{103}Rh [50], ^{159}Tb [51], ^{169}Tm [8], and ^{175}Lu [48] targets, ^{12}C induced reaction with ^{103}Rh [52], ^{159}Tb [20], ^{169}Tm [53], and ^{175}Lu [48] targets, ^{13}C induced reaction with ^{159}Tb [20], ^{169}Tm [37], and ^{175}Lu [54] targets at a constant relative velocity ($V_{rel} = 0.053c$) and are presented in Fig. 10. The dotted lines are drawn to guide the eyes for an individual projectile. This figure clearly shows that the ICF fraction increases almost linearly with increasing mass asymmetry but separately for each projectile with different targets. The present observation shows that Morgenstern's mass-asymmetry systematic [27] does not explain the variation of $F_{ICF}(\%)$ with μ_A for a given projectile target system. However, more ICF probability is found for the projectile ^{18}O induced reactions than ^{16}O , ^{12}C , and ^{13}C induced reactions with the same target nuclei. This indicates that the projectile structure, along with the mass asymmetry of the projectile-target combination plays an important role in ICF reactions at these low energies. Further, the present results are in a good manner with the projectile-dependent mass-asymmetry systematics reported by Singh *et al.* [8].

C. ICF dependence on Coulomb factor ($Z_P Z_T$)

The variation of the ICF fraction $F_{ICF}(\%)$ with respect to the Coulomb factor parameter which is the product ($Z_P Z_T$) has also been studied at the same relative velocity ($V_{rel} = 0.053c$)

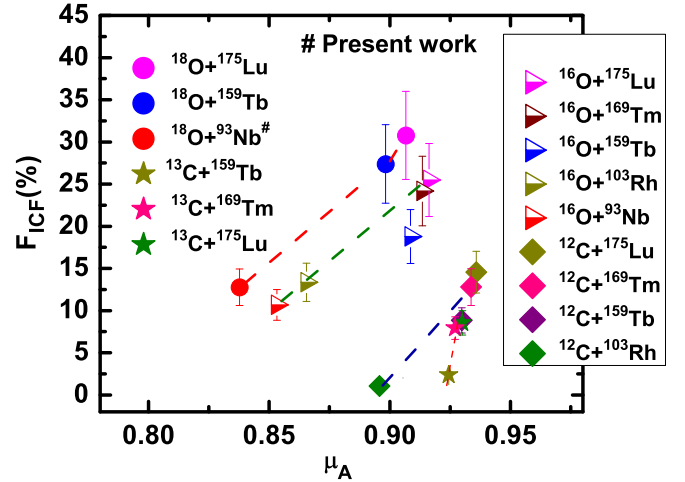


FIG. 10. Comparison of deduced $F_{ICF}(\%)$ of the $^{18}\text{O} + ^{93}\text{Nb}$ system with earlier studied systems as a function of entrance channel mass asymmetry (μ_A) at same relative velocity ($V_{rel} = 0.053c$). The lines drawn are just to guide the eye. For references and details see text.

and is found to influence the ICF systematics (see Fig. 11). The systems and their symbols are the same as those in Fig. 10. Recently, Shuaib *et al.* [28] have observed that the $F_{ICF}(\%)$ may also be influenced by the product of projectile and target charges, i.e., $Z_P Z_T$ and found a linear dependence

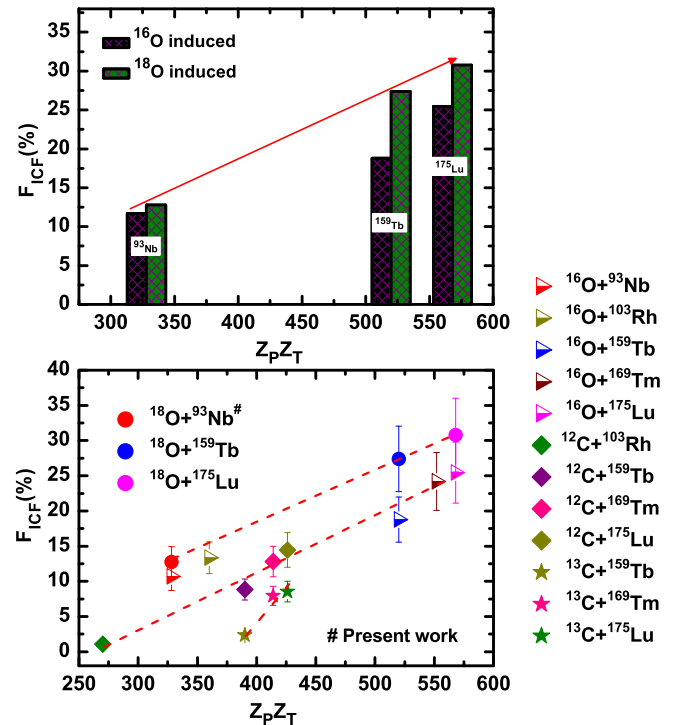


FIG. 11. The $F_{ICF}(\%)$ deduced from the present system along with those obtained for earlier studied systems as a function of Coulomb factor ($Z_P Z_T$) at the same relative velocity ($V_{rel} = 0.053c$). The color lines drawn through the data points are just to guide the eyes. For references and details see text.

of $F_{ICF}(\%)$ with the Coulomb factor parameter ($Z_P Z_T$). Moreover, it is quite interesting to see that $F_{ICF}(\%)$ values for ^{12}C and ^{16}O (α cluster structured) projectile induced reactions follow a linear dependence with increasing parameter $Z_P Z_T$ and lie on the same line but in the case of ^{18}O and ^{13}C (non- α -cluster structured), the $F_{ICF}(\%)$ values also follow a same linear trend with increasing parameter $Z_P Z_T$, but separately for each projectile. Highest $F_{ICF}(\%)$ values are observed for ^{18}O while lowest $F_{ICF}(\%)$ values are observed for ^{13}C . The present observations reveal that the Coulomb factor ($Z_P Z_T$) governs the ICF up to some extent. The present result is found to be consistent with the recently observed similar findings [29,30]. For the projectiles having the same Z_P numbers (like ^{12}C - ^{13}C and ^{16}O - ^{18}O) with the target of the same Z_T , the ICF dependence with the Coulomb factor could not be explained. As such, the discrepancy observed in the $Z_P Z_T$ influence on ICF using the projectiles like ^{12}C - ^{13}C and ^{16}O - ^{18}O with the same target may be understood more clearly in terms of the ground state Q value of the reaction.

D. ICF dependence on neutron skin thickness

The neutron skin thickness (t_N) is a residual property of nuclei which appears mainly in heavy nuclei due to the unequal number of neutrons and protons. In heavy nuclei, the numbers of neutrons are found to be more as compared to the numbers of protons which results in the formation of neutron skin on its surface. Since, ICF reactions at low incident energies are mainly surface dominated, it would be interesting to study the effect of neutron skin thickness on the onset and strength of ICF. The neutron skin thickness may be defined as the difference between matter radius (R_m) and charge radius (R_c) of a nucleus, i.e., $t_N = (R_m - R_c)$ [31,55]. The value of t_N may be calculated as [56]

$$t_N = \frac{2}{3} r_0 A^{1/3} (I - \delta),$$

where, A is the mass number of the target nuclei, I is a factor define $\frac{(N-Z)}{A}$, and δ represents the density dependent factor [56]. The ICF fraction for the present system $^{18}\text{O} + ^{93}\text{Nb}$ has been compared with those obtained for ^{18}O induced reactions with ^{159}Tb [4] and ^{175}Lu [48] targets and ^{16}O induced reactions with ^{93}Nb [49], ^{103}Rh [50], ^{159}Tb [51], and ^{175}Lu [48] targets as a function of neutron skin thickness is shown in Fig. 12. An interesting trend is observed from this figure, the value of ICF fraction increases with t_N , indicating the ICF dependence on neutron skin thickness. This may be because neutron skin thickness slightly reduces the Coulomb potential and increases the attractive nuclear potential of the target which influences the probability of CF and give a way to ICF process to proceed. It may be pointed out that $F_{ICF}(\%)$ increases with t_N for individual projectiles. This suggests that ^{18}O having two excess neutrons in its structure must have larger ICF probability which has been also observed in our study.

E. ICF dependence on ground state Q value of reaction

In recent studies [20,28,32], the probability of incomplete fusion has been discussed in terms of projectile α -separation

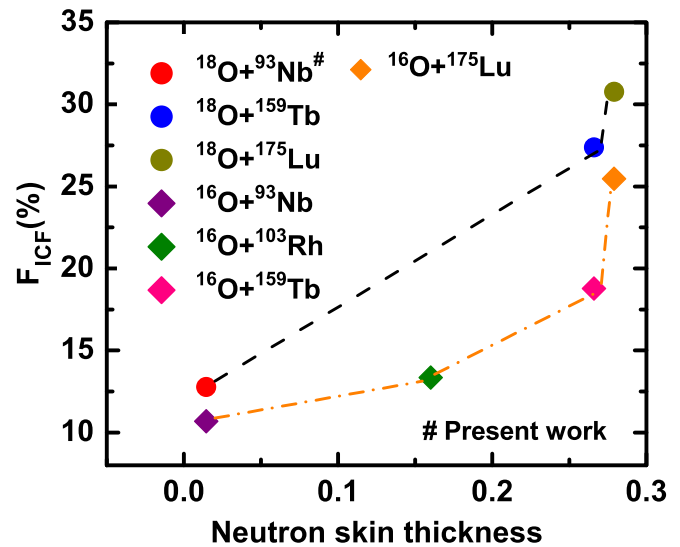


FIG. 12. The variation of incomplete fusion fraction with neutron skin thickness (t_N) at relative velocity, $V_{\text{rel}} = 0.053c$. For references and details see text.

energy. It has been noticed that the value of the ICF fraction is found to be less for larger negative α -separation energies. Most nuclear reactions are studied by the properties of both projectile and target nuclei. Therefore, the properties of both projectile and target nuclei should be taken into consideration while interpreting the method of incomplete fusion. In the present work, the probability of ICF has been observed as a function of ground state Q value (Q_{gs}) of reaction to incorporate the properties of both projectile and target nuclei. The Q_{gs} value of the reaction is defined as the mass difference between incident and exit channels. In order to see the effect of this parameter on ICF more clearly, reactions induced by different projectiles ^{18}O , ^{16}O , ^{13}C , and ^{12}C with ^{93}Nb , ^{103}Rh , ^{159}Tb , ^{169}Tm , and ^{175}Lu targets have been studied. The ground state Q value of these reactions along with the percentage of ICF fraction at a constant relative velocity ($V_{\text{rel}} = 0.053c$) is presented in Table IV. As can be seen from Table IV, the percentage ICF fraction is more for projectile ^{18}O in comparison to other projectiles ^{16}O , ^{12}C , and ^{13}C . This suggests that the larger negative Q_{gs} value may be responsible for the projectile breakup leading to the onset of ICF. Moreover, this paper shows the strong projectile structure dependence of ICF for α - and non- α -clustered projectiles with the same target. Thus, reaction Q_{gs} values seem to be an important entrance channel parameter, which may explain the projectile structure effect more effectively.

F. Effect of neutron excess on ICF dynamics

As discussed in earlier sections, the onset of the ICF contribution is found to be reasonably different for $^{18}\text{O} + ^{93}\text{Nb}$ and $^{16}\text{O} + ^{93}\text{Nb}$ systems, that may be due to the effect of two additional neutrons in ^{18}O as compared to the ^{16}O projectile. For a better understanding of the projectile structure dependence of ICF the radii of ^{18}O and ^{16}O have been calculated using standard relation $R = R_0 A^{1/3}$ (keeping $R_0 = 1.2$ fm) and

TABLE IV. The ground state Q value ($Q_{g.s.}$) and $F_{ICF}(\%)$ of ^{18}O , ^{16}O , ^{13}C , and ^{12}C induced reactions with different targets at a constant relative velocity ($V_{\text{rel}} = 0.053c$).

System	$Q_{g.s.}$	$F_{ICF}(\%)$
Projectile: ^{18}O		
^{93}Nb	-2.01	12.78
^{159}Tb	-15.85	27.39
^{175}Lu	-19.92	30.78
Projectile: ^{16}O		
^{93}Nb	-7.30	11.68
^{103}Rh	-8.19	13.35
^{159}Tb	-18.86	18.78
^{169}Tm	-21.92	24.18
^{175}Lu	-22.78	25.47
Projectile: ^{13}C		
^{159}Tb	-7.51	2.35
^{169}Tm	-9.98	7.93
^{175}Lu	-10.24	8.54
Projectile: ^{12}C		
^{103}Rh	-2.06	1.05
^{159}Tb	-9.41	8.84
^{169}Tm	-11.98	12.80
^{175}Lu	-11.78	14.55

are found to be ≈ 3.145 fm and 3.023 fm, respectively. It is important to note that as such no justified relationship of ICF with projectile size could be obtained. The ^{18}O projectile has two excess neutrons resulting in rather weak binding forces as compared to ^{16}O having a larger probability of breakup. Following the neutron excess in the projectile ^{18}O , the contribution of ICF is expected to be more as compared to the ^{16}O projectile. The effect of projectile structure on ICF dynamics has been demonstrated in Fig. 13. The fact is that ^{18}O is weakly bound as compared to ^{16}O and has larger probability to break, resulting in more ICF contribution, as expected.

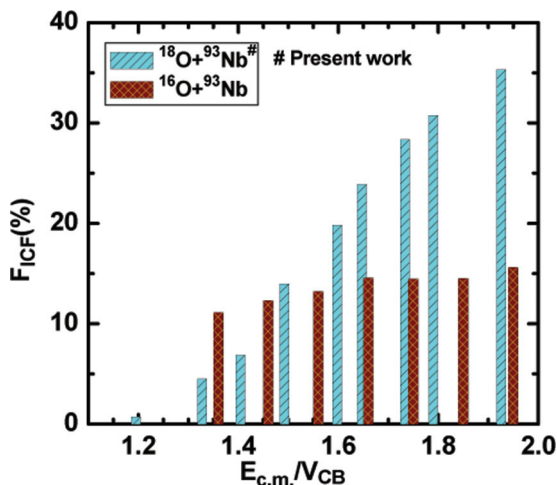


FIG. 13. Comparison of deduced $F_{ICF}(\%)$ as a function of normalized projectile energy for $^{18}\text{O}+^{93}\text{Nb}$ and $^{16}\text{O}+^{93}\text{Nb}$ systems.

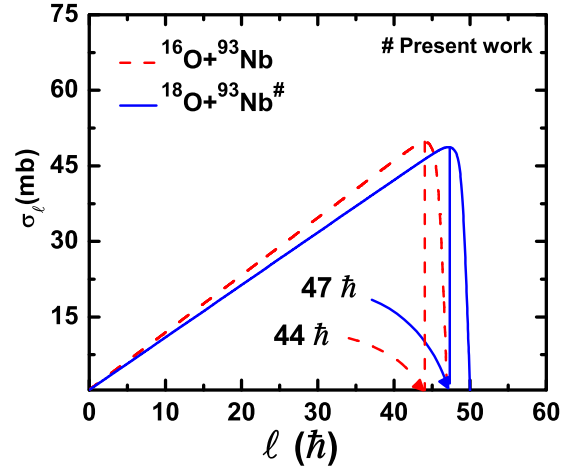


FIG. 14. Fusion l distributions for the $^{18}\text{O}+^{93}\text{Nb}$ and $^{16}\text{O}+^{93}\text{Nb}$ [49] systems calculated using the CCFULL code [58] and by incorporating the coupled-channel calculations at ≈ 99.20 MeV energy.

G. Observation of ICF below critical angular momentum

An attempt has been made to explore the role of input angular momentum (l) in the study of ICF reaction dynamics. Trautmann *et al.* [11] suggest that ICF reactions are related to peripheral collisions. As per the sharp cutoff approximation of the SUMRULE model [10], the ICF probability is assumed to exist for $l > l_{\text{crit}}$ and to be zero for $l \leq l_{\text{crit}}$. According to Wilczynski [57], the value of l_{crit} for a colliding system can be estimated from the equilibrium condition of the Coulomb, nuclear, and centrifugal forces as

$$\pi(\gamma_1 + \gamma_2) \frac{R_1 R_2}{R_1 + R_2} = \frac{Z_1 Z_2 e^2}{(R_1 + R_2)^2} + \frac{l_{\text{crit}}(l_{\text{crit}} + 1)\hbar^2}{\mu(R_1 + R_2)^3}$$

where R_1 and R_2 are the half-density radii and μ is the reduced mass of the binary system. The value of l_{crit} estimated using the above formulation for the $^{18}\text{O}+^{93}\text{Nb}$ and $^{16}\text{O}+^{93}\text{Nb}$ [49] systems are found to be $54\hbar$ and $50\hbar$, respectively. However, the maximum angular momentum (l_{max}) calculated using the CCFULL code [58] is estimated to be $47\hbar$ and $44\hbar$, respectively, at the highest incident energy ≈ 99.2 MeV. The fusion l distribution for $^{18}\text{O}+^{93}\text{Nb}$ and $^{16}\text{O}+^{93}\text{Nb}$ systems have been calculated by using the code CCFULL at the same energy and is displayed in Fig. 14. The calculations are done without considering any coupling between the interacting partners. It is due to the fact that coupling plays an important role at energies near and below the barriers. This figure shows clearly that the l_{max} value is less than the l_{crit} value at the studied energy. However, a substantial ICF contribution has been observed at this energy. This comparison also supports the ICF existence below critical angular momentum (l_{crit}), i.e., l_{crit} for $^{18}\text{O}+^{93}\text{Nb}$ and $^{16}\text{O}+^{93}\text{Nb}$ systems. Hence, it is inferred that a number of collision trajectories having values $l \leq l_{\text{crit}}$ contribute significantly to ICF. The present findings clearly indicate that the fusion l -distribution window approached by the SUMRULE model [10] is a broadly diffused boundary.

V. SUMMARY AND CONCLUSION

The excitation functions of several reaction residues formed by complete and incomplete fusion in the $^{18}\text{O} + ^{93}\text{Nb}$ system above barrier energies have been studied using the offline γ ray spectroscopy method. An attempt has been made to deduce the independent cross section of ^{105}Ag residue fed by their higher charge isobar. The experimentally measured EFs have been compared with PACE4 predictions. It has been found that EFs of all xn and/or pxn channels are well reproduced in the PACE4 predictions with level density parameter $a = A/12 \text{ MeV}^{-1}$, implying the population of these ERs by the CF process. However, the enhancement has been found for α -emitting channels for the same set of input parameters, which is attributed to the ICF process. Moreover, the dependence of the ICF reaction for the different parameters, i.e., projectile energy, entrance channel mass asymmetry, the Coulomb factor, ground state Q value, and neutron skin thickness, has been studied for a large number of projectile-target combinations. It has been found that the probability of ICF increases with incident energy. The increasing trend of the ICF fraction with mass asymmetry has been observed, which increases separately for each projectile with different targets. It is quite interesting to see that the system having the same values of $Z_p Z_T$ show large ICF fraction for ^{18}O rather than the ^{16}O induced reaction with the same targets. Further, it has been also observed that the probability of ICF is likely to be effected by neutron skin thickness and ground state α - Q value. The probability of ICF increases with negative ground state α - Q value of the reaction and neutron skin thickness

for individual projectiles. The reason may be that the neutron skin thickness and ground state α - Q value of the reaction are proportional to the target mass. More interestingly ICF contribution for the two neutron excess projectile ^{18}O as compared to ^{16}O is noticed to be relatively larger, that may be due to the larger probability of breakup for the ^{18}O projectile with two neutron excess resulting in rather weak binding forces as compared to ^{16}O . Moreover, the present results show the occurrence of ICF at $\ell > \ell_{\text{crit}}$, which suggests that a refinement in the basic assumption of the SUMRULE model is needed at low incident energies.

ACKNOWLEDGMENTS

The authors are thankful to the Director IUAC, New Delhi, for providing all the necessary facilities to carry out the experiment. One of the authors, A.A., is thankful to Science and Engineering Research Board (SERB)-Department of Science and Technology (DST), New Delhi, India for financial support through research Project No. EMR/2016/006983. Thanks are also due to Dr. Manoj K. Sharma for reading the manuscript and giving valuable suggestions. The authors also extend their gratitude towards Dr. V. P. Singh, Head Physics Department, and Dr. Anuraag Mohan, Principal, Bareilly College, Bareilly (India) for their support and interest in this work. Thanks also are due to Target Laboratory, especially Abhilash S. R., and technical staff of Pelletron Laboratory for providing the uninterrupted and stable beam during the experiment.

-
- [1] S. Hofmann *et al.*, *Euro. Phys. J. A* **32**, 251 (2007); **14**, 147 (2002).
- [2] V. I. Zagrebaev, *Nucl. Phys. A* **734**, 164 (2004).
- [3] L. Corradi *et al.*, *Nucl. Phys. A* **734**, 237 (2004).
- [4] A. Yadav *et al.*, *EPJ Web Conf.* **117**, 08022 (2016).
- [5] P. R. S. Gomes, R. Linares, J. Lubian, C. C. Lopes, E. N. Cardozo, B. H. F. Pereira, and I. Padron, *Phys. Rev. C* **84**, 014615 (2011).
- [6] D. J. Parker, J. J. Hogan, and J. Asher, *Phys. Rev. C* **39**, 2256 (1989).
- [7] D. R. Zolnowski, H. Yamada, S. E. Cala, A. C. Kahler, and T. T. Sugihara, *Phys. Rev. Lett.* **41**, 92 (1978).
- [8] P. P. Singh, B. P. Singh, M. K. Sharma, Unnati, D. P. Singh, R. Prasad, R. Kumar, and K. S. Golda, *Phys. Rev. C* **77**, 014607 (2008).
- [9] H. C. Britt and A. R. Quinton, *Phys. Rev.* **124**, 877 (1961).
- [10] J. Wilczynski, K. Siwek-Wilczynska, J. van Driel, S. Gonggrijp, D. C. J. M. Hageman, R. V. F. Janssens, J. Lukasiak, and R. H. Siemssen, *Phys. Rev. Lett.* **45**, 606 (1980).
- [11] W. Trautmann, O. Hansen, H. Tricoire, W. Hering, R. Ritzka, and W. Trombik, *Phys. Rev. Lett.* **53**, 1630 (1984).
- [12] T. Inamura, T. Kojima, T. Nomura, T. Sugitate, and H. Utsunomiya, *Phys. Lett. B* **84**, 71 (1979).
- [13] T. Inamura, A. C. Kahler, D. R. Zolnowski, U. Garg, T. T. Sugihara, and M. Wakai, *Phys. Rev. C* **32**, 1539 (1985).
- [14] T. Udagawa and T. Tamura, *Phys. Rev. Lett.* **45**, 1311 (1980).
- [15] J. P. Bondrop, J. N. De, G. Fai, A. O. T. Karvinen, and J. Randrup, *Nucl. Phys. A* **333**, 285 (1980).
- [16] M. Blann, *Phys. Rev. C* **31**, 295(R) (1985).
- [17] K. Kumar, T. Ahmad, S. Ali, I. A. Rizvi, A. Agarwal, R. Kumar, K. S. Golda, and A. K. Chaubey, *Phys. Rev. C* **87**, 044608 (2013).
- [18] M. Kumar, A. Agarwal, S. Prajapati, K. Kumar, S. Dutt, I. A. Rizvi, R. Kumar, and A. K. Chaubey, *Phys. Rev. C* **100**, 034616 (2019).
- [19] D. P. Singh, Unnati, P. P. Singh, A. Yadav, M. K. Sharma, B. P. Singh, K. S. Golda, R. Kumar, A. K. Sinha, and R. Prasad, *Phys. Rev. C* **80**, 014601 (2009).
- [20] A. Yadav, V. R. Sharma, P. P. Singh, R. Kumar, D. P. Singh, Unnati, M. K. Sharma, B. P. Singh, and R. Prasad, *Phys. Rev. C* **86**, 014603 (2012).
- [21] S. Dutt, A. Agarwal, M. Kumar, V. R. Sharma, I. A. Rizvi, R. Kumar, and A. K. Chaubey, *EPJ Web Conf.* **66**, 03024 (2014).
- [22] S. Dutt, A. Agarwal, M. Kumar, K. Kumar, I. A. Rizvi, R. Kumar, and A. K. Chaubey, *EPJ Web Conf.* **86**, 00009 (2015).
- [23] D. Kumar and M. Maiti, *Phys. Rev. C* **96**, 044624 (2017).
- [24] R. Prajapat and M. Maiti, *Phys. Rev. C* **101**, 024608 (2020).
- [25] D. Kumar, M. Maiti, and S. Lahiri, *Phys. Rev. C* **96**, 014617 (2017).
- [26] S. B. Linda, Ph.D. thesis, Central University of Jharkhand, Ranchi, India, 2018.
- [27] H. Morgenstern, W. Bohne, W. Galster, K. Grabisch, and A. Kyanowski, *Phys. Rev. Lett.* **52**, 1104 (1984).

- [28] Mohd. Shuaib *et al.*, *Phys. Rev. C* **94**, 014613 (2016).
- [29] S. A. Tali *et al.*, *Nucl. Phys. A* **970**, 208 (2018).
- [30] H. Kumar *et al.*, *Euro. Phys. J. A* **54**, 47 (2018).
- [31] Tamii *et al.*, *Phys. Rev. Lett.* **107**, 062502 (2011).
- [32] V. R. Sharma *et al.*, *Phys. Rev. C* **89**, 024608 (2014).
- [33] R. Tripathi, K. Sudarshan, S. Sodaye, S. K. Sharma, A. V. R. Reddy, and A. Goswami, *Eur. Phys. J. A* **42**, 25 (2009).
- [34] S. Sodaye, K. Sudarshan, B. S. Tomar, A. Goswami, S. Mukherjee, and K. Mahata, *Eur. Phys. J. A* **14**, 371 (2002).
- [35] R. Tripathi, K. Sudarshan, S. Sodaye, and A. Goswami, *J. Phys. G: Nucl. Part. Phys.* **35**, 025101 (2008).
- [36] P. P. Singh *et al.*, *Phys. Lett. B* **671**, 20 (2009).
- [37] D. Singh *et al.*, *Phys. Lett. B* **774**, 7 (2017).
- [38] A. Gavron, *Phys. Rev. C* **21**, 230 (1980).
- [39] B. P. Ajith Kumar, E. T. Subramaniam, K. Singh, and R. K. Bhowmik, DAE-BRNS Nuclear Physics Symposium, Kolkata, 2001 (unpublished), <http://www.iuac.res.in/NIAS/>.
- [40] The Stopping and Range of Ions in Matter (SRIM) code, <http://www.srim.org/SRIM/SRIMLEGL.htm>.
- [41] E. Browne and R. B. Firestone, *Table of Radioactive Isotopes* (Wiley, New York, 1986).
- [42] A. Agarwal, I. A. Rizvi, R. Kumar, B. K. Yogi, and A. K. Chaubey, *Int. J. Mod. Phys. E* **17**, 393 (2008).
- [43] W. Hauser and H. Feshbach, *Phys. Rev.* **87**, 366 (1952).
- [44] R. Bass, *Phys. Rev. Lett.* **39**, 265 (1977).
- [45] M. Maiti, *Phys. Rev. C* **84**, 044615 (2011).
- [46] H. H. Gutbrod, W. G. Winn, and M. Blann, *Phys. Rev. Lett.* **30**, 1259 (1973).
- [47] M. Cavinato, E. Fabrici, E. Gadioli, E. Gadioli Erba, P. Vergani, M. Crippa, G. Colombo, I. Redaelli, and M. Ripamonti, *Phys. Rev. C* **52**, 2577 (1995).
- [48] H. Kumar, Ph.D. thesis, Aligarh Muslim University, 2017.
- [49] A. Sharma, B. B. Kumar, S. Mukherjee, S. Chakrabarty, B. S. Tomar, A. Goswami, and S. B. Manohar, *J. Phys. G: Nucl. Part. Phys.* **25**, 2289 (1999).
- [50] U. Gupta, P. P. Singh, D. P. Singh, M. K. Sharma, A. Yadav, R. Kumar, B. P. Singh, and R. Prasad, *Nucl. Phys. A* **811**, 77 (2008).
- [51] M. K. Sharma, Unnati, B. P. Singh, R. Kumar, K. S. Golda, H. D. Bhardwaj, and R. Prasad, *Nucl. Phys. A* **776**, 83 (2006).
- [52] B. B. Kumar, A. Sharma, S. Mukherjee, S. Chakrabarty, P. K. Pujari, B. S. Tomar, A. Goswami, S. B. Manohar, and S. K. Datta, *Phys. Rev. C* **59**, 2923 (1999).
- [53] P. P. Singh *et al.*, *J. Phys. Conf. Ser.* **282**, 012019 (2011).
- [54] H. Kumar *et al.*, *Phys. Rev. C* **99**, 034610 (2019).
- [55] S. Abrahamyan *et al.*, *Phys. Rev. Lett.* **108**, 112502 (2012).
- [56] W. D. Myers, *Phys. Lett. B* **30**, 451 (1969).
- [57] J. Wilczynski, *Nucl. Phys. A* **216**, 386 (1973).
- [58] K. Hagino, N. Rowley, and A. T. Kruppa, *Comput. Phys. Commun.* **123**, 143 (1999).